Available online at www.sciencedirect.com

SciVerse ScienceDirect

Ceramics International 38 (2012) 5799–5805

CERAMICS INTERNATIONAL

www.elsevier.com/locate/ceramint

Microstructure and mechanical properties of 3-D interpenetrated network structure $MoSi_2$–RSiC composite

Peng-zhao Gao *, Ling Wang, Shi-ting Huang, Wen-ming Guo, Wen Xie, Han-ning Xiao

College of Materials Science and Engineering, Hunan University, Changsha 410082, China

Received 1 November 2011; received in revised form 9 April 2012; accepted 10 April 2012
Available online 16 April 2012

Abstract

In this paper, RSiC is used as matrix, organic precursor impregnation and pyrolysis – $MoSi_2$ melt infiltration combined processes are employed to prepare the 3-D interpenetrated network structure $MoSi_2$–RSiC composite. The composition, microstructure and mechanical properties of $MoSi_2$–RSiC composite are studied through XRD, SEM, EDS and mechanical testing. The results show that an almost fully dense $MoSi_2$–RSiC composite with 3-D interpenetrated network structure is obtained. The main components of the composite are SiC and $MoSi_2$, it also includes small amount of $Mo_{4.8}Si_3C_{0.6}$. The flexural strength of $MoSi_2$–RSiC composite is improved compared with that of RSiC, meanwhile, it inherits the high temperature strength characteristic from RSiC. The composite exhibits a typical brittle fracture behavior and the elastic modulus of it also increases with the increase of organic precursor impregnation and pyrolysis cycles.

Keywords: $MoSi_2$–RSiC; 3-D interpenetrated network structure; Flexural strength; Elastic modulus

1. Introduction

Molybdenum disilicide ($MoSi_2$) is widely used as a high-temperature electrical-heating material for its excellent high temperature oxidation resistance and thermal conductivity (45 W/m K). But its low-temperature brittleness and poor high temperature creep resistance lead to poor reliability and short service life in actual applications [1].

Re-crystallized silicon carbide (RSiC) maintains excellent creep resistance and high strength at elevated temperatures. It has been widely used for bearing parts in air above 1400 °C [2]. In addition, RSiC is also used as a thermal exchanger and particulate filter material at elevated temperatures because of its high thermal conductivity coefficient (20–30 W/m K), relatively low coefficient of thermal expansion (C_{TE}, 4.8–5.2 $\times 10^{-6}$ K^{-1}) and good wear resistance [3–5]. As we know that RSiC does not exhibit any shrinkage during its re-crystallized process because of the evaporation–condensation mechanism of sintering. This results in a 3-D interconnected porous microstructure of RSiC [2]. The porous structure of RSiC is severely detrimental to its properties, such as high temperature oxidation resistance, mechanical, thermal and electrical properties. Consequently, the porous structure reduces the service life and confines the application fields of RSiC [6].

Recently, a new type of ceramic-metal composite, in which both phases are continuous and three-dimensionally interpenetrating in the whole microstructure, is attracting much attention. This type of composite mimics many natural materials such as bone and bamboo. It presents multifunctional characteristics with each phase contributing its own properties; the microstructure and properties also exhibit an isotropic behavior. The most general method of fabricating the composite is to impregnate a desired second phase into the pre-existing open-cell porous preform, which can produce the requisite connectivity and spatial distribution of the two or more component phases [7–9].

The main purpose of this study is to combine the excellent performance of RSiC with that of $MoSi_2$ to prepare a 3-D interpenetrated network structure $MoSi_2$–RSiC composite. In this composite, $MoSi_2$ is used to improve the oxidation resistance and electrical properties, while RSiC is used as the skeleton for its excellent creep resistance and high strength at elevated temperatures. The anticipated composite should

* Corresponding author. Tel.: +86 731 88822269; fax: +86 731 88823554.
E-mail address: gaopengzhao7602@hnu.edu.cn (P.-z. Gao).

0272-8842/$36.00.
http://dx.doi.org/10.1016/j.ceramint.2012.04.027

possess excellent mechanical, electrical and thermal properties. It should also have good oxidation and creep resistance at elevated temperatures in oxide atmosphere.

In this paper, organic precursor impregnation-prolysis (PIP) and $MoSi_2$ melting-infiltration (MI) combined processes are used to prepare a 3-D interpenetrated network structure $MoSi_2$–RSiC composite. The PIP process is used to adjust the porous structure and density of RSiC matrix, while MI process is used to transfer the melting $MoSi_2$ into RSiC. The influence of PIP cycles on the microstructure and mechanical properties of composite is studied through XRD, SEM, EDS and mechanical testing.

2. Experimental procedures

2.1. Raw materials

RSiC is prepared according the procedure in Ref. [2], the flexural strength of it is 82.0 MPa (RT) and porosity of it is equal to 23.7%. Polycarbosilane (PCS) powder is used as raw material for the PIP process; the average molecular weight of it is 1400–200. Its soften point equals to 220 °C and is obtained from National University of Defense Technology, China. The $MoSi_2$ powder is employed as raw material for melt infiltration. Its purity exceeds 99.5%, D_{50} of it equals to 6.09 μm and is obtained from Zhengzhou Songshan Heating Elements Co. Ltd., Zhengzhou, China.

2.2. Preparation of $MoSi_2$–RSiC composite

The PIP process is performed to obtain RSiC with a range of porosities and densities through controlling cycles when raw RSiC is used as preform according to the procedure in Ref. [10]. Afterwards, RSiC samples with different porosities and densities are used as matrix, the MI process is conducted at 2100 °C for 1 h in graphite crucible in an argon protective atmosphere using $MoSi_2$ powder as the infiltration agent [2]. The serial numbers of samples are shown in Table 1.

2.3. Characterization of RSiC and $MoSi_2$–RSiC materials

The volume density and apparent porosity of RSiC and $MoSi_2$–RSiC materials are measured using Archimedes method.

The phase identification of RSiC and $MoSi_2$–RSiC materials is performed by X-ray diffraction (XRD, Rigaku D/max2200 VPC) using monochromic Cu Kα radiation of 0.15405 nm operated at 40 kV and 40 mA.

The morphology of RSiC and $MoSi_2$–RSiC materials is observed using a scanning electron microscope (ESEM, FEI Quanta 200) equipped with an energy dispersive spectrometer (EDS).

The flexural strength of RSiC and $MoSi_2$–RSiC materials is measured at room temperature and at an elevated temperature of 1400 °C with three-point bending method on specimens having dimensions of 4 mm × 4 mm × 40 mm. The specimens are ground with diamond wheels and the tensile surfaces are polished to a finish better than 1 μm. The edges are beveled to avoid stress concentration effects during testing. A batch of six specimens is tested at two temperatures for each kind of the materials. The tests are carried out at a cross-head speed of 0.5 mm min^{-1} in a GKZ-II servohydraulic testing machine equipped with a split furnace attachment for conducting the high-temperature test. The heating rate for the high-temperature test is 5 °C min^{-1} with a soaking time of 15 min at the test temperature to facilitate temperature in homogeneity prior to carrying out the test. The following equation is used to calculate the flexural strength of composite:

$$\sigma_f = \frac{3FL}{2bh^2} \quad (1)$$

where σ_f stands for flexural strength, F for maximum load at sample fracture, L for the distance between the outer load points, b for width of sample and h for height of sample.

3. Results and discussion

3.1. Phase characterization of RSiC and $MoSi_2$–RSiC materials

The respective XRD patterns of RSiC and $MoSi_2$–RSiC materials are shown in Fig. 1. Compared with standard spectra of SiC and $MoSi_2$, it is easy to see that the main composition of RSiC is 6H-SiC. As for the $MoSi_2$–RSiC, the main composition is 6H-SiC and $MoSi_2$. Specimens also include a small amount of $Mo_{4.8}Si_3C_{0.6}$, which is derived from the reaction of $MoSi_2$ and SiC according to Ref. [11].

Table 1
Serial numbers of samples.

Preparation process	PIP process					MI process				
Composition	RSiC					$MoSi_2$–RSiC				
Cycle times	0	1	2	3	4	1	1	1	1	1
Serial number	0#	1#	2#	3#	4#	0-1#	1-1#	2-1#	3-1#	4-1#

* 0#, 1#, 2 #, 3# and 4 # stand for the RSiC with different porosity and density, which are obtained by controlling the PIP cycles. For example: 0 # stands for the raw RSiC; 1 # stands for the material that raw RSiC is used as matrix and PIP process is performed once; The rest samples are named similarly like the abovementioned. * 0-1#, 1-1#, 2-1 # 3-1# and 4-1 # stand for $MoSi_2$–RSiC composite with different composition and density, which are obtained by PIP and MI combined processes. For example: 0-1# stands for the composite that raw RSiC is used as matrix and then MI process is performed. 1-1# stands for the composite that 1 # sample is used as matrix and then MI process is performed. The rest samples are named similarly like the abovementioned.

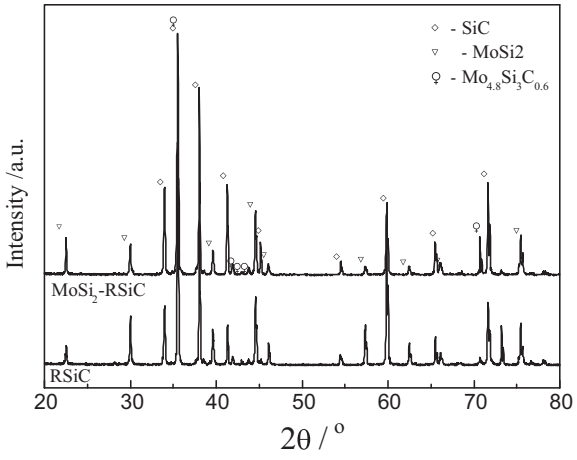

Fig. 1. XRD patterns of RSiC and $MoSi_2$–RSiC materials.

3.2. Apparent porosity and volume density of RSiC and $MoSi_2$–RSiC materials

Curves of apparent porosity and volume density of RSiC and $MoSi_2$–RSiC materials versus PIP cycles are shown in Fig. 2. From Fig. 2a, it can be seen clearly that with the increase of PIP cycles, the apparent porosity of RSiC decreases while that of density increases for the pyrolytic SiC derived from PIP filling in the pores of RSiC.

From Fig. 2b, it can be seen that with the increase of PIP cycles, the apparent porosity of $MoSi_2$–RSiC did not change significantly; all data are close to 3%. While the density of composite decreases. As we know, $MoSi_2$ exhibits excellent wetting with SiC at temperature above its melting point (2030 °C) [2]; hence, it can easily infiltrate into the RSiC matrix and fill in the pores through capillary action. Thus, an almost fully dense $MoSi_2$–RSiC composite is obtained. But a great difference exists between the theoretic density of SiC (3.2 g m^{-3}) and $MoSi_2$ (6.5 g cm^{-3}) [12]. With the increase of PIP cycles, the porosity of RSiC decreases (Fig. 2a), which leads to a decrease in the volume fraction of $MoSi_2$ in the $MoSi_2$–RSiC composite, as expected after the MI process. Consequently, the density of $MoSi_2$–RSiC decreases.

Namely, an almost full density $MoSi_2$–RSiC composite is obtained, which helps to improve the oxidation resistance of the composite at elevated temperatures. The influence of PIP cycles on the oxidation resistance of composite will be discussed next.

3.3. Influence of PIP cycles on the microstructure of RSiC and $MoSi_2$–RSiC materials

3.3.1. Influence of PIP cycles on the microstructure of RSiC material

Cross-section SEM photographs of RSiC with a different number of PIP cycles are shown in Fig. 3. From Fig. 3a and b, we can see that RSiC material exhibits a typical 3-D interconnected porous structure. As in Fig. 3d and f, it can be seen clearly that the pyrolytic SiC derived from PIP process exists on the surface of RSiC particle and combines well with particle surface [13]. With the increase of PIP cycles, the amount of pyrolytic SiC increases.

3.3.2. Influence of PIP cycles on the microstructure of $MoSi_2$–RSiC material

Cross-section SEM photographs of the $MoSi_2$–RSiC composite with a different number of PIP cycles are shown in Fig. 4 (the gray part can be interpreted as SiC and the white part as $MoSi_2$). From the figure, we can see that the $MoSi_2$–RSiC composite exhibits a typical 3-D interconnected network structure. Both SiC and $MoSi_2$ phases are continuous and three-dimensionally interpenetrating through the entire body of the composite. The SiC and $MoSi_2$ phase combines very well without any observable pores or cracks.

Interface line scanning EDS spectra of the $MoSi_2$–RSiC composite with a different number of PIP cycles are shown in Fig. 5 (red line is normalized for carbon content, green line for silicon content, blue line for Mo content). From Fig. 5a, we can find a clear interface between SiC and $MoSi_2$; no elemental diffusion is detected. While for the sample 2-1# (Fig. 5b), it exhibits a compact interface regime with some Mo diffusing into the RSiC matrix. The main reason for this observation is that pyrolytic SiC derived from PIP process is more active than that from RSiC. The pyrolytic SiC can react easily with $MoSi_2$ to produce a $Mo_{4.8}Si_3C_{0.6}$ phase. The compact interface combination of SiC and $MoSi_2$ in composite can help to improve the properties of the composite, such as oxidation

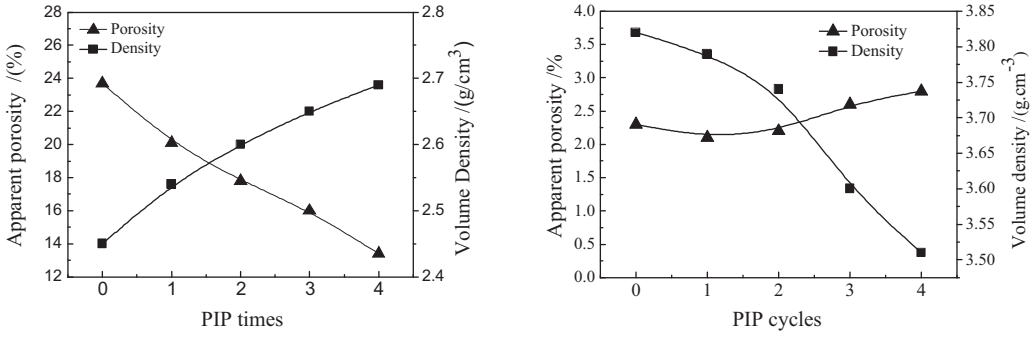

(a) RSiC (b) $MoSi_2$-RSiC

Fig. 2. Curves of porosity and density of RSiC and $MoSi_2$–RSiC materials versus PIP cycles.

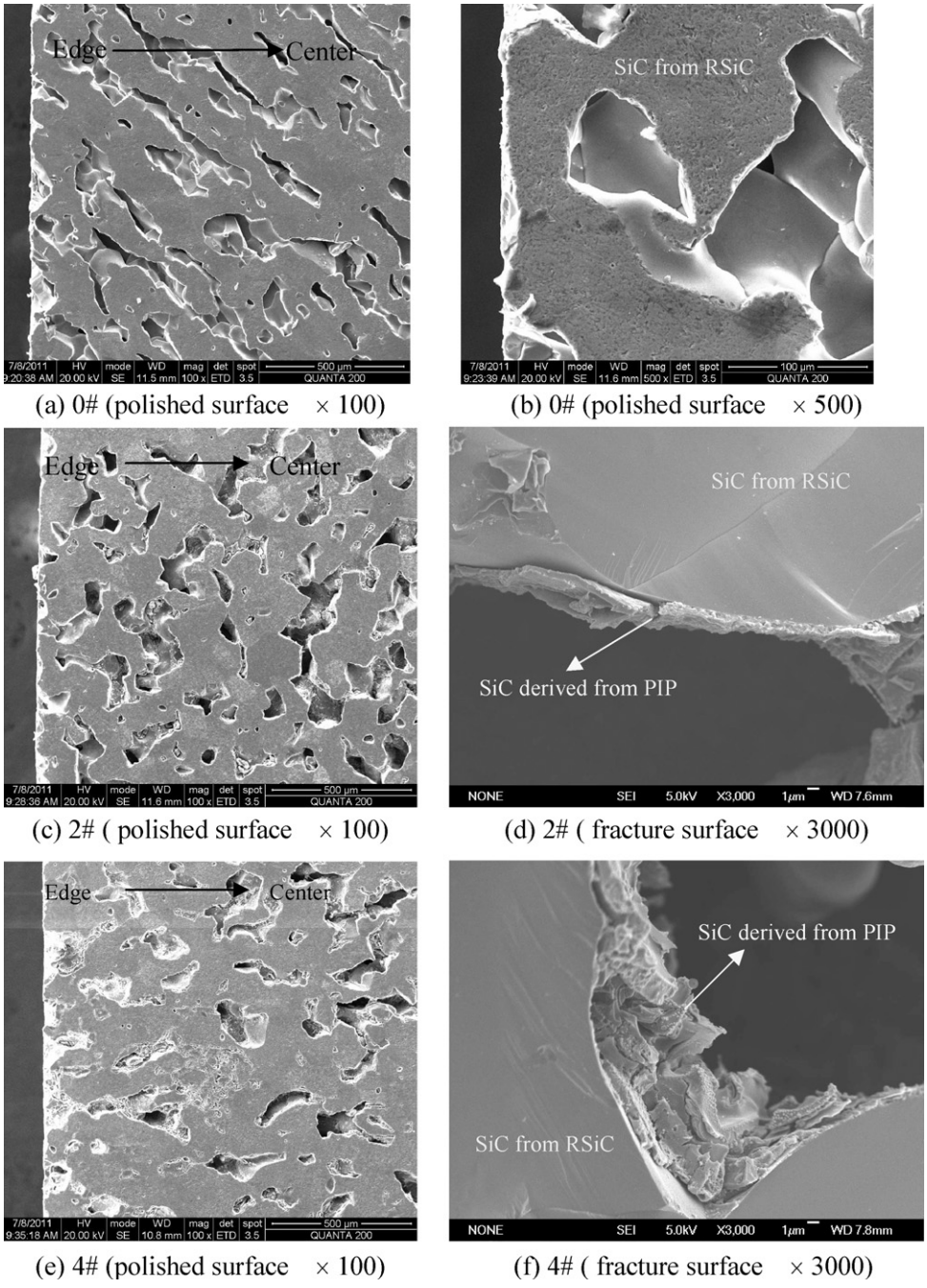

Fig. 3. Cross-section SEM photographs of RSiC with a different number of PIP cycles.

resistance, electrical, thermal and mechanical properties. These will be discussed next.

3.4. Influence of PIP cycles on the mechanical properties of RSiC and $MoSi_2$–RSiC materials

Curves of flexural strength of RSiC and $MoSi_2$–RSiC materials versus PIP cycles are shown in Fig. 6. From the figure, we can see it clearly that with the increase of PIP cycles, all the flexural strengths of RSiC and $MoSi_2$–RSiC materials increase.

As for RSiC materials, with the increase of PIP cycles, more and more pyrolytic SiC fills into the pore of RSiC matrix. This helps to increase the bearing area during loading process, so the strength of RSiC materials increases.

As for $MoSi_2$–RSiC composite, we can see that all measured strengths are higher than that of RSiC. Besides, with the increase of PIP cycles, the strength of the composite further increases. As we know the coefficient of thermal expansion (C_{TE}) mismatch of SiC and $MoSi_2$ ($4.8–5.2 \times 10^{-6}\ K^{-1}$ for SiC and $8.1 \times 10^{-6}\ K^{-1}$ for $MoSi_2$) [12] makes a negative effect on the mechanical properties when the material need to be served in a range of temperature. While in the current case, resulting MoSiC phase by interface reaction can work as a C_{TE} coupling buffer. With the increase of PIP cycles, more and more

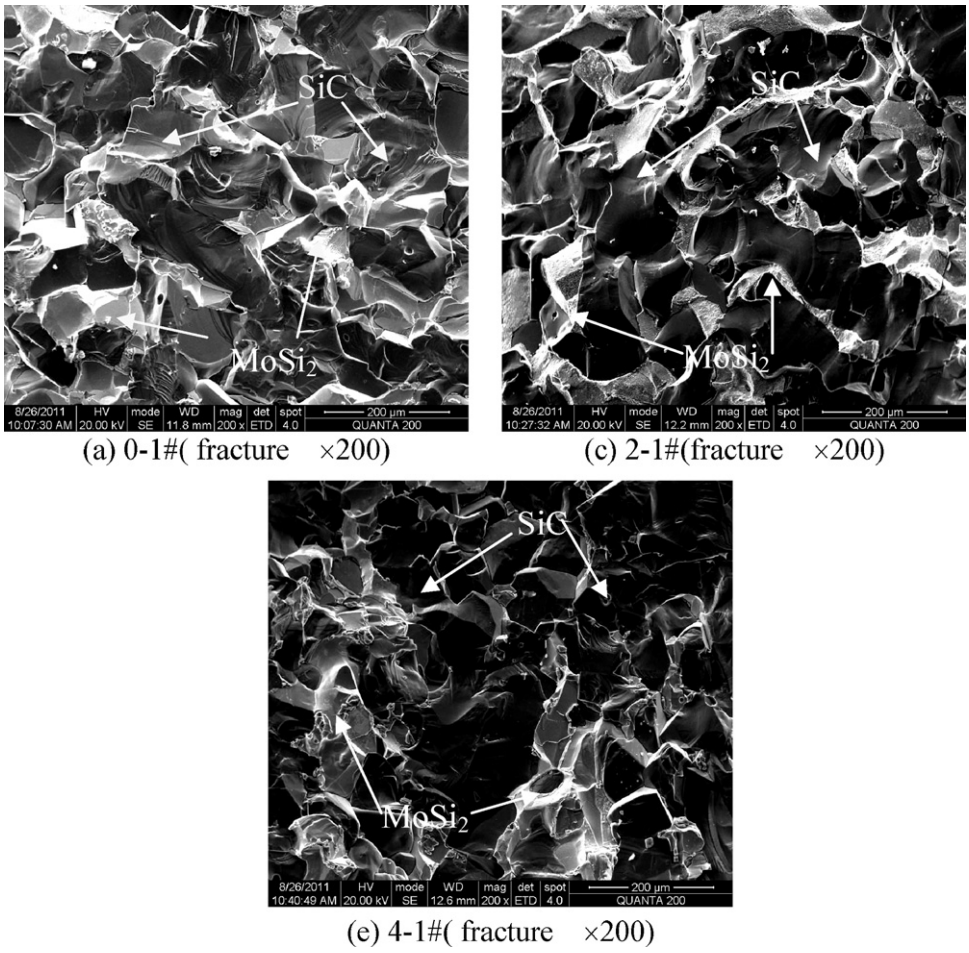

Fig. 4. Cross-section SEM photographs of the $MoSi_2$–RSiC composite with a different number of PIP cycles.

pyrolytic SiC deposited on RSiC particle surface, which in term resulting a thicker $Mo_{4.8}Si_3C_{0.6}$ C_{TE} buffer layer during MI process. Finally, it leads to the increase of flexural strength of the composite [11].

From Fig. 6, it also can be seen clearly that the composite strength at 1400 °C increases with increase of PIP cycle. Also compared with the data measured at room temperature, its strength increases by about 10–15%. This observation is similar to the typical strength characteristic of the RSiC material that the strength increases with the increase of operation temperature. Namely, the strength of the $MoSi_2$–RSiC composite behaves in the same manner as RSiC material and it should prove to be a useful material as bearing parts at temperature above 1400 °C as that of the RSiC materials.

Compared with widely used reaction-bonded SiC (RBSiC), the $MoSi_2$–RSiC exhibits a poor flexural strength

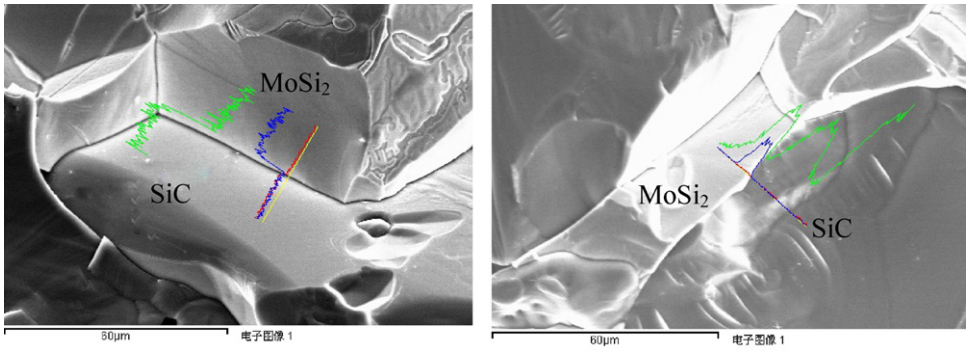

Fig. 5. Interface line scanning EDS spectra of the $MoSi_2$–RSiC with a different number of PIP cycles. (For interpretation of the references to color in text, the reader is referred to the web version of the article.)

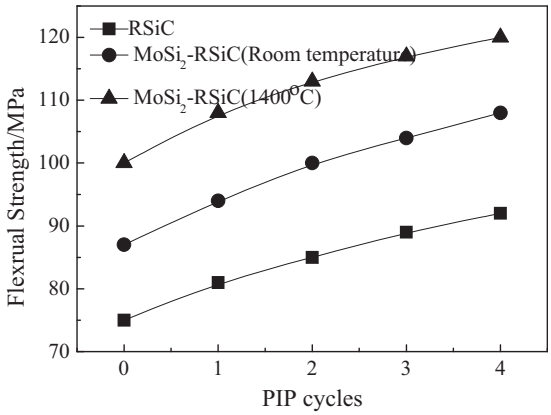

Fig. 6. Curves of flexural strength of RSiC and $MoSi_2$–RSiC materials versus PIP cycles.

at low temperature. The strength of the $MoSi_2$–RSiC composite at room temperature is equal to about 108 MPa while that of RBSiC is equal to about 350 MPa. However, the strength of $MoSi_2$–RSiC at 1400 °C is better than that of RBSiC: 120 MPa compared to 80 MPa. In addition, the strength of RBSiC decreases swiftly with increase of operation temperature [14].

The stress–strain curves of RSiC and $MoSi_2$–RSiC materials with a different number of PIP cycles are shown in Fig. 7. From the figure, we can see that all curves exhibit a typical brittle fracture behavior. The elastic modulus of these samples can be calculated from the slope of corresponding curves. That is 210 GPa for 0#, 245 GPa for 0-1#, 260 GPa for 2-1# and 266 GPa for 4-1#.

From the data, it can be seen clearly that with the increase of PIP cycles, the elastic modulus of composite also increases in some extent for the same reason as the strength change of $MoSi_2$–RSiC composite.

4. Conclusions

(1) An almost fully dense $MoSi_2$–RSiC composite with 3-D interpenetrated network structure is obtained. The phases of the composite are mainly SiC and $MoSi_2$. A small amount of $Mo_{4.8}Si_3C_{0.6}$ is also present and is believed to be derived from the reaction of SiC and $MoSi_2$;

(2) The flexural strength of $MoSi_2$–RSiC composite is improved compared with that of RSiC. Also, with the increase of PIP cycles, the strength of the composite increases, for the pyrolytic SiC derived from PIP can react with $MoSi_2$ to produce the $Mo_{4.8}Si_3C_{0.6}$ buffer layer between SiC and $MoSi_2$ interface, it helps to decrease the mismatch of C_{TE} between SiC and $MoSi_2$ to improve the strength of composite;

(3) The $MoSi_2$–RSiC composite retains the typical high temperature strength characteristic of RSiC, namely, it's strength increases with the increase of operation temperature. So it can serve as bearing parts at elevated temperature as RSiC material;

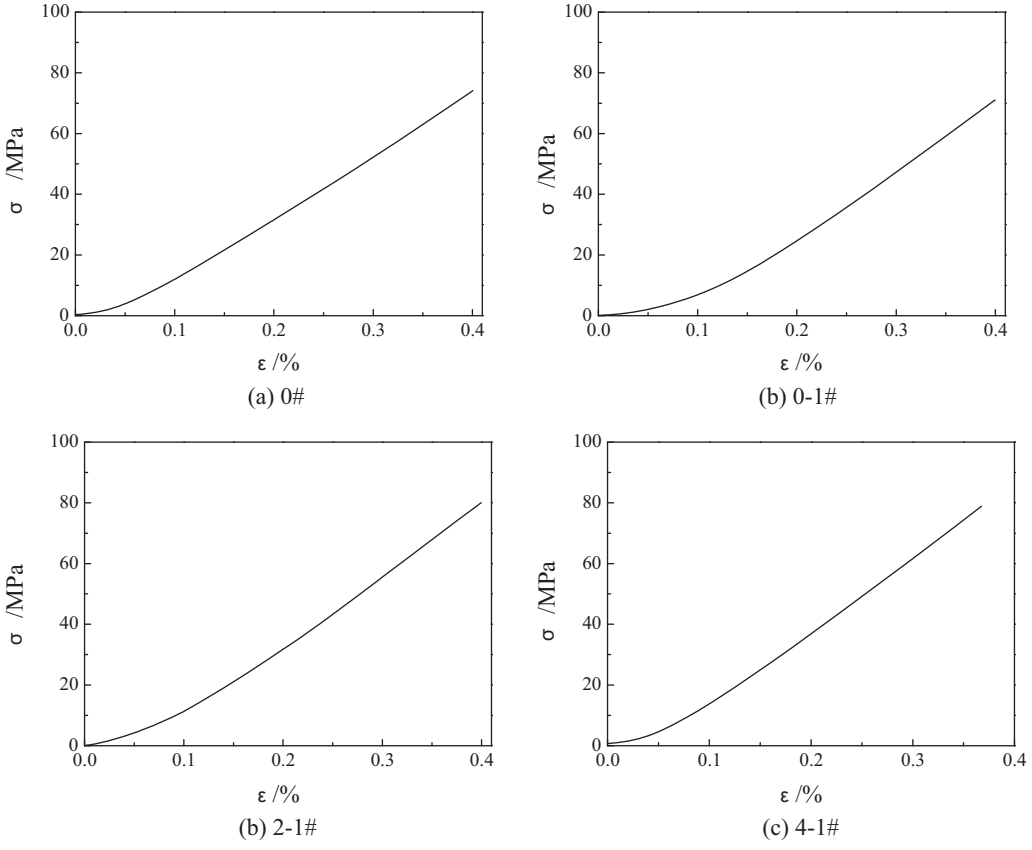

Fig. 7. Stress–strain curves of RSiC and $MoSi_2$–RSiC materials with a different number of PIP cycles.

(4) The composite exhibits a typical brittle fracture behavior and the elastic modulus of the composite also increases with the increase of PIP cycles.

Acknowledgements

This work are supported by National Natural Science Foundation of China (Grant No. 50972042) and State Key Laboratory for Mechanical Behavior of Materials (Grant No. 20111202).

References

[1] K. Peng, M. Yi, L. Ran, Y. Ge, Effect of the W addition content on valence electron structure and properties of $MoSi_2$-based solid solution alloys, Materials Chemistry and Physics 129 (2011) 990–994.
[2] W. Guo, H. Xiao, P. Gao, W. Xie, Q. Li, J. Hu, Investigation of $MoSi_2$ melt infiltrated RSiC and its oxidation behavior, Ceramics International 38 (2012) 111–117.
[3] N. Orlovskaja, H. Peterlik, W. Steinkellner, K. Kromp, Prediction of strength of re-crystallized silicon carbide from pore size measurement: part 1. The bimodality of the distribution [J], Journal of Materials Science 35 (2000) 699–705.
[4] Z.Z. Yi, Z.P. Xie, Y. Huang, J.T. Ma, Y.B. Cheng, Study on gel-casting and properties of recrystallized silicon carbide, Ceramics International 28 (2002) 369–376.
[5] C.C. Agraiotis, I. Mavroidis, A.G. Konstandopoulos, B. Hoffschmidt, P. Stobbe, M. l Romerod, V. Fernandez-Queroe, Evaluation of porous silicon carbide monolithic honeycombs as volumetric receivers/collectors of concentrated solar radiation, Solar Energy Materials and Solar Cells 91 (2007) 474–488.
[6] A. Sonntag, New R-SiC extends service life in kiln furniture, American Ceramic Society Bulletin 76 (1997) 51–54.
[7] J. Winzer, L. Weiler, J. Pouquet, Wear behavior of interpenetrating alumina–copper composites, Wear 271 (2011) 2845–2851.
[8] C.N. He, F. Tian, A carbon nanotube–alumina network structure for fabricating epoxy composites, Scripta Materialia 61 (2009) 285–288.
[9] Z. Guo, G. Blugan, T. Graule, M. Reeceb, J. Kuebler, The effect of different sintering additives on the electrical and oxidation properties of Si_3N_4–$MoSi_2$ composites, Journal of the European Ceramic Society 27 (2007) 2153–2161.
[10] G. Wenming, X. Hanning, L. Haibo, X. Wen, Densification of re-crystallized Silicon carbide prepared by precursor-impregnation and pyrolysis process, Kuei Suan Jen Hsueh Pao 38 (8) (2010) 1514–1518.
[11] Q. Zhu, K. Shobu, SiC–$Mo_{\leq 5}Si_{\leq 3}C_{\leq 1}$ composites by melt infiltration process, Journal of Materials Science 19 (2000) 153–155.
[12] X. Hanning, G. Pengzhao, Advance structural ceramic and its application, Chemistry & Industry Pre (2006) 5.
[13] S.-a. Chen, H.-f. Hu, Y.-d. Zhang, X.-b. He, M. Mei, Rapid densification of C/SiC composites by joint processes of CLVD and PIP, Materials Letters 65 (2011) 37–39.
[14] Q.-W. Huang, L.-H. Zhu, High-temperature strength and toughness behaviors for reaction-bonded SiC ceramics below 1400 °C, Materials Letters 59 (2005) 1732–1735.